

Initial electron donor and acceptor in isolated Photosystem II reaction centers identified with femtosecond mid-IR spectroscopy

Marie Louise Groot^{††}, Natalia P. Pawlowicz[†], Luuk J. G. W. van Wilderen[†], Jacques Breton[§], Ivo H. M. van Stokkum[†], and Rienk van Grondelle[†]

[†]Faculty of Sciences, Vrije Universiteit, 1081 HV, Amsterdam, The Netherlands; and [§]Service de Bioénergétique, Bât. 532, Commissariat à l'Énergie Atomique-Saclay, 91191 Gif-sur-Yvette, France

Edited by Pierre A. Joliot, Institut de Biologie Physico-Chimique, Paris, France, and approved July 19, 2005 (received for review April 27, 2005)

Despite the apparent similarity between the plant Photosystem II reaction center (RC) and its purple bacterial counterpart, we show in this work that the mechanism of charge separation is very different for the two photosynthetic RCs. By using femtosecond visible-pump-mid-infrared probe spectroscopy in the region of the chlorophyll ester and keto modes, between 1,775 and 1,585 cm^{-1} , with 150-fs time resolution, we show that the reduction of pheophytin occurs on a 0.6- to 0.8-ps time scale, whereas P^+ , the precursor state for water oxidation, is formed after ≈ 6 ps. We conclude therefore that in the Photosystem II RC the primary charge separation occurs between the “accessory chlorophyll” Chl_{D1} and the pheophytin on the so-called active branch.

electron transfer | photosynthesis | pump-probe

The primary steps of energy and electron transfer in green plants' photosynthesis occur in two large protein complexes called Photosystem I and Photosystem II (PSII). PSII is an aggregate of many individual pigment-protein complexes. The core of PSII consists of the chlorophyll (Chl)-binding antenna-proteins CP43 and CP47, which feed excitation energy into the $\text{D}_1\text{D}_2\text{cytb559}$ reaction center (RC). Crystal structures of PSII cores from cyanobacteria have been resolved with increasingly high resolution (1–3); currently, the resolution is 3.2 Å (4). The structure of the PSII RC shows four Chls and two pheophytins (H) arranged in two branches very similar to the bacterial RC. In the heart of the PSII RC, there is a dimer of Chls, and in each branch there is one monomeric Chl and one H. Furthermore, there are two distant Chls bound to the periphery of the PSII RC. Although the structure suggests there may be a “special pair” of strongly electronically coupled pigments in the PSII RC, the visible absorption spectrum does not show a distinct band. This finding is in contrast to the bacterial RC, where the lowest energy absorption band fully originates from one of the exciton transitions of a special pair of bacteriochlorophylls.

Since the first purification of the PSII RC in 1987 (5), it has been speculated that its way of operation would be similar to that of the bacterial RC, with a special pair that upon excitation drives a charge separation in ≈ 3 ps. This idea was based on the strong homology between the bacterial RC and the PSII RC, the strong similarity in the pigment composition, even details in the way the pigments interacted with the protein, and the near-identity of the electron transfer events at the acceptor side. Conversely, it was clear that major differences between the two RCs had to exist at the electron donor side where in the PSII RC charge separation eventually leads to the oxidation of water and the production of molecular oxygen, requiring a very large oxidation potential of the primary electron donor (>1.2 V vs. 0.45 V in the bacterial RC).

In the mid-1990s, it was recognized that energy transfer and charge separation in the PSII RC most likely proceeded in a manner that is very different from that in the bacterial RC. The “spectroscopic absence” of a special pair and the fact that in the

PSII RC the Hs absorb light in the same spectral region as the Chls led to the proposal of the “multimer” model (6), in which the interactions between all of the chlorins are about equal, and consequently the excitation may get localized on any of the chlorins, depending on the specific realization of the disorder. This model was used to interpret the spectroscopic data of the PSII RC (6) and later the dynamics of energy and electron transfer (7, 8).

Excitation of the PSII RC with a short laser flash leads to ultrafast charge separation followed by the formation of the radical pair $\text{P}_{\text{D1}}^+\text{H}_{\text{D1}}^-$, consisting of the H molecule in the D_1 branch, H_{D1} , and one of the Chl forming the special pair, P_{D1} (9). Electron transport stops at the H molecule because the final quinone acceptors are missing in these preparations. In contrast to the bacterial RC, in the PSII RC the initial dynamics are highly multiexponential with lifetimes in the order of 100 and 300–400 fs, and 3, 10, and 30 ps (7, 10–18). These dynamics all seem to represent a mixture of energy transfer, excited state decay, radical pair-formation and relaxation, in part due to the shallow equilibria between the excited pigments and the initial radical pair state(s). These observations and the difficulty in identifying the intrinsic charge separation rate (7, 10–18) undoubtedly reflect the fact that the kinetics in the PSII RC are intrinsically complicated, but in part they are due to the difficulty in disentangling contributions from energy and electron transfer, because of the extensively overlapping pigment absorption bands in the PSII RC combined with the intrinsic heterogeneity of biological systems.

Recently, it has been suggested by several groups that the “accessory” Chl on the D_1 branch is the true primary electron donor in the PSII RC and that electron transfer starts with formation of the pair $\text{Chl}_{\text{D1}}^+\text{H}_{\text{D1}}^-$ for the following reasons: (i) in analogy with the alternative electron transfer pathways in bacterial RCs (19–21), (ii) on the basis of its proposed red absorption (22), (iii) its proposed oxidation potential (23), (iv) the strong H Stark signal interpreted as a charge transfer state $\text{Chl}_{\text{D1}}^+\text{H}_{\text{D1}}^-$ (24), and (v) analysis of photon echo data (25). How charge separation is initiated between the pigments in the PSII RC at the microscopic level, and whether pigments other than P_{D1} and H_{D1} play a role in early radical pair intermediates, is, however, clearly difficult to resolve when using visible spectroscopy. In principle, the observation of the rate of P_{D1} oxidation and H_{D1} reduction should be more straightforward when analyzing the large manifold of vibrational bands afforded by

This paper was submitted directly (Track II) to the PNAS office.

Freely available online through the PNAS open access option.

Abbreviations: Chl, chlorophyll; H, pheophytin; PSII, Photosystem II; RC, reaction center; EADS, evolution associated difference spectra; THF, tetrahydrofuran.

^{††}To whom correspondence should be addressed at: Faculty of Sciences, Vrije Universiteit, De Boelelaan 1081, 1081 HV, Amsterdam, The Netherlands. E-mail: ml.groot@few.vu.nl.

© 2005 by The National Academy of Sciences of the USA

mid-IR spectroscopy (although at the cost of much lower extinction coefficients), because the spectra of Chl and H in their anion, cation, and neutral states have very specific signatures in the mid-IR (26–31). We therefore performed visible pump/mid-IR probe spectroscopy on isolated RCs of PSII at room temperature. Our data show the ultrafast reduction of H on a time scale very different from that of P oxidation.

Materials and Methods

D₁D₂-Cyt-b559 RC complexes were isolated from spinach as described in ref. 32. Anaerobic conditions were achieved by bubbling the D₂O buffer solution (pH 6.5) with argon gas for 2 h. The samples were concentrated to an OD of 0.2 per 20 μ m at 675 nm. Approximately 40 μ l of RC solution was put in a closed cell consisting of two CaF₂ plates separated by a 20- μ m spacer. The cell then was placed in the setup, which was contained in a flow box purged with N₂. Samples were kept in the dark at all times. Chl *a* was purchased from Sigma and dissolved in tetrahydrofuran (THF) or prepared with an excess of trifluoroacetic acid to form pheophytin *a*.

The experimental setup consists of a Ti:sapphire amplified laser system operating at 1 kHz (Hurricane, Spectra-Physics), producing pulses of 0.65 mJ with a duration of 85 fs. This laser system is used to pump a collinear optical parametric amplifier of superfluorescence (TOPAS, Light Conversion, Vilnius, Lithuania) equipped with difference frequency generator, producing pulses at 1,680 cm^{-1} with a $\approx 200\text{-cm}^{-1}$ bandwidth. Another part of the Hurricane output was used to pump a home-built noncollinear optical parametric amplifier. The visible excitation and the mid-IR probe pulses were attenuated and focused onto the sample with a 200- and 60-mm lens, respectively. The probe pulses were dispersed onto a spectrograph after the sample and imaged onto a 32-element mercury-cadmium-tellurium detector array, yielding a spectral resolution of 5.9 cm^{-1} . The absorption of a polystyrene film was used for spectral calibration of the setup. The sample was continuously moved in a home-built Lissajous scanner, ensuring the excitation of a fresh spot at every shot. Pump and probe polarizations were set at the magic angle (54.7°). The cross-correlation of visible and mid-IR pulses was measured in GaAs to be 150 fs.

Excitation was at 681 nm (full width at half-maximum = 8 nm) and 669 nm (full width at half-maximum = 9 nm) using 240 or 80 nJ of excitation power. In the latter case, the kinetics were the same as with 240 nJ, and the signals were accordingly smaller, showing that excitation was in the linear regime. For one excitation wavelength, two or three data sets were collected, taking 30 min each, on two freshly prepared RC samples. After a check for consistency, the five data sets were averaged. Data analysis was performed by using global and target analysis methods (33). Because no reference probe pulse was used, the noise in the measured spectra consists mainly of so-called baseline noise, i.e., a flat, structureless offset in the spectra, which is easily recognized by a singular vector decomposition of the residual matrix. For target analysis (and the time traces in Fig. 1), the outer product of the first two singular vector pairs of the residual matrix (being structureless in the time domain) was subtracted from the data, leading to reduction in the noise by a factor of 2.

Results

Excitation at 669 nm. Three representative time traces measured at 1,657, 1,681, and 1,711 cm^{-1} upon excitation of the PSII RC at 669 nm are shown in Fig. 1. The lines through the data are a fit with time constants of 0.2, 3, and 32 ps, 2 ns, a nondecaying component, and a component that follows the instrument response instantaneously. The latter describes the coherent interaction of the laser pulses in the sample and will not be discussed further here. All time traces collected in the region of

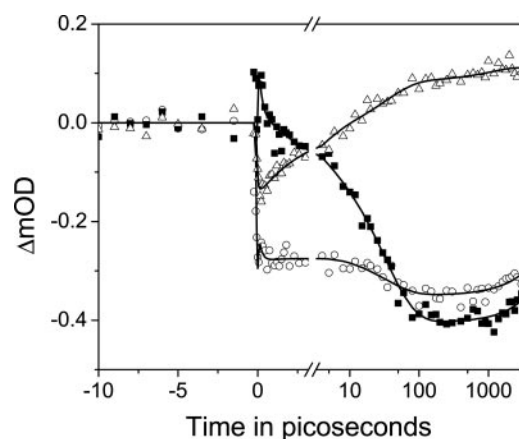


Fig. 1. Time traces at 1,657 (■), 1,681 (○), and 1,711 (△) cm^{-1} upon excitation at 669 nm. The solid line through the data points is a fit with $t_1 = 0.2$ ps, $t_2 = 3$ ps, $t_3 = 32$ ps, $t_4 = 2$ ns, and $t_5 = \text{infinite}$; instrument response is 150 fs. The time scale is linear up to 3 ps and logarithmic thereafter. The rms error of the fit is 15 μOD .

1,775–1,585 cm^{-1} are well fitted with these five time constants. Fig. 2 shows the spectral evolution of the time-dependent absorption changes when fitted to a sequential model (state1 \rightarrow state2 \rightarrow state3 \rightarrow state4 \rightarrow state5) yielding so-called evolution associated difference spectra (EADS) (33).

In the difference spectra, we observe the bleaching of several keto C₉=O stretches of either Chl or H molecules between 1,710 and 1,640 cm^{-1} . The exact frequency of the keto stretch of a Chl or H molecule depends on whether or not it has a hydrogen bond and on the polarity of its environment. The stronger the hydrogen bond, or the larger the polarity of the environment, the lower the frequency of the C₉=O mode. The bleached bands change in amplitude and shift in time, indicating the bleaching of different (sets of) Chl and H molecules as energy and electron transfer occur (Fig. 2). The absorption difference signal at early times is overall positive between 1,670 and 1,635 cm^{-1} ; we attribute this part of the spectrum to the keto C₉=O stretch of Chl and H molecules in the excited state, because a similar shift to lower frequencies was observed for the excited state of Chl molecules in the CP47 antenna complex (34) and in THF (in which Chl is in a nonhydrogen-bonded form) the keto stretch of

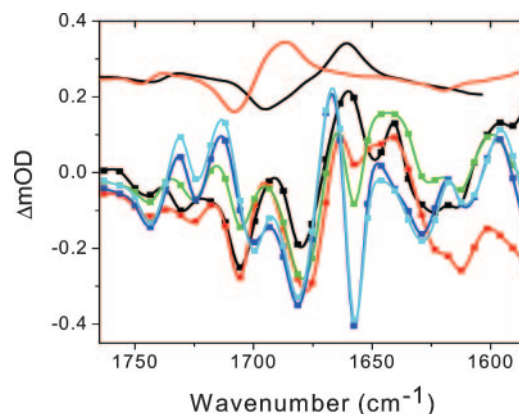


Fig. 2. Lower curves show the evolution of the time-dependent absorption changes in the PSII RC upon 669-nm excitation. The lifetimes of the spectra are 0.2 ps (black), 3 ps (red), 32 ps (green), 2 ns (blue), and infinite (cyan). A smooth line is drawn through the measuring points as a guide for the eye. The Chl*/Chl (black line) and H*/H (red line) difference spectra in THF measured 10 ps after excitation at 530 nm are shown (upper curves) for comparison.

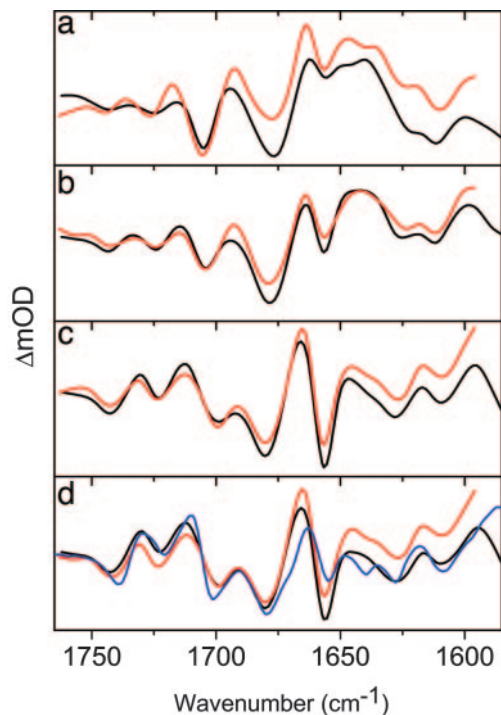


Fig. 3. EADS upon 669-nm (black lines) and 681-nm excitation (red lines). The lifetimes of the spectra are 3 and 0.6 ps (a); 32 and 21 ps (b), 2 ns and 500 ps (c); infinite and infinite (d), for the 669- and 681-nm data sets, respectively. In d, the $P^+H_{D1}^-$ spectrum from steady-state Fourier transform IR experiments (blue line) is reproduced from refs. 27 and 30 for comparison.

Chl*/Chl downshifts from 1,695 to 1,660 cm^{-1} (see Fig. 2, upper spectrum). The keto stretch of the Chl cation upshifts $\approx 25 \text{ cm}^{-1}$ with respect to the neutral form, to 1,718 cm^{-1} in THF (26), and for the PSII RC the P^+/P spectrum has been reported to have positive peaks at 1,729–1,724 and 1,711 cm^{-1} (27, 28, 31). Therefore, the peak that appears at 1,713 cm^{-1} in Fig. 2 may be tentatively interpreted as the rise of the spectrum P^+/P .

The 10a-ester band of Chl and H absorbs in the 1,710–1,750 cm^{-1} region. In the excited state, the ester band of Chl in CP47 downshifts from 1,737 to 1,726 cm^{-1} (34). The ester band of Chl* and Pheo* in THF downshift $\approx 8 \text{ cm}^{-1}$ (see Fig. 2, upper spectra), whereas for Chl in the cation state, in THF, the band upshifts from 1,738 to 1,751 cm^{-1} (26). These ester modes are quite weak because the ester is less conjugated with the π electron system than the keto group. The H_{D1}^-/H_{D1} difference spectrum measured in PSII, conversely, shows two strong negative bands at 1,739 and 1,722 cm^{-1} due to the 10a-carbomethoxy ester C=O group of the molecule (29–31). The strong, typical, H_{D1}^-/H_{D1} bands seem to be present in the absorbance difference spectra already on an early time scale, especially in the spectra upon 681-nm excitation (see Fig. 3).

Excitation at 681 nm. The dynamics upon 681-nm excitation in the region 1,775–1,590 cm^{-1} (for a selection of transient spectra, see Fig. 6, which is published as supporting information on the PNAS web site) are fitted with time constants of 0.6, 21, and 500 ps and a nondecaying component; the corresponding EADS are compared with those obtained upon 669-nm excitation in Fig. 3. We compare the 0.6-ps EADS with the 3-ps spectrum of the 669-nm data set, because the 0.2-ps 669-nm spectrum has a bleaching at 1,649 cm^{-1} (Fig. 2) and not at 1,657 cm^{-1} . The presence of this fast component upon 669-nm excitation is in good agreement with the reported time scale for exciton equilibration of ≈ 100 –300 fs (7, 10, 12, 13). Most likely, we do not resolve this

component upon 681-nm excitation because the amplitude is expected to be smaller than that upon 669 nm, according to a Boltzmann population distribution (with $\Delta E \sim 220 \text{ cm}^{-1}$, $k_B T \sim 200 \text{ cm}^{-1}$, the ratio is ≈ 0.3). From the relatively close agreement between the 3-ps, 669-nm EADS and the 0.6-ps, 681-nm EADS, we conclude that the 0.2-ps equilibration process leads to a population similar to that obtained upon 681-nm excitation, but notably not identical, because the amplitude of the bleaching at 1,656–1,657 cm^{-1} is clearly larger on this time scale upon 681-nm excitation (Fig. 3a), and so are the features at $>1,700 \text{ cm}^{-1}$. Because of the width of the excitation pulses, the 669- and 681-nm excitations cannot be considered completely selective, which contributes to the similarity of the spectra. We note that the time constants of 0.6 and 21 ps are in good agreement with those we have found earlier at 240 K in visible pump–probe experiments (i.e., 0.4 and 18 ps), which we assigned to direct charge separation and energy transfer limited charge separation (15).

In Fig. 3d, we compare the two longest-lived EADS with the sum of P^+/P and H_{D1}^-/H_{D1} spectra obtained by steady-state Fourier transform IR techniques (27, 30). There is clearly very good agreement between our nanosecond spectra and the steady-state $P^+H_{D1}^-$ spectrum. The P^+/P and H_{D1}^-/H_{D1} spectra reported by Noguchi *et al.* (31) suggest an even higher degree of similarity because their H_{D1}^-/H_{D1} spectrum shows a large amplitude of the 1,664/1,657 cm^{-1} bandshift, similar to that in our H_{D1}^-/H_{D1} spectrum. The magnitude of this band depends on temperature and varies even somewhat from experiment to experiment (J.B., unpublished results). Raman spectra of PSII RCs do not show any bands between 1,660 and 1,640 cm^{-1} (28), and therefore the 1,664/1,657- cm^{-1} bandshift is probably due to an amide C=O response to the charge separation, rather than to a Chl keto. Both the P^+/P and the H_{D1}^-/H_{D1} spectra have a band in this region [at 1,653–1,655 and 1,657 cm^{-1} , respectively (27–31)] for which a similar origin has been suggested before (28, 31).

Discussion

The mid-IR difference spectra are clearly very rich in formation. The longest-lived spectrum shows an excellent agreement with the steady-state $P^+H_{D1}^-/PH_{D1}$ spectrum, and the multiexponential decay times of the earlier absorption-difference spectra are in good agreement with the time constants observed in visible pump–probe experiments. The early time spectra most likely represent equilibria among excited states, between excited states and radical pair states, and among radical pair states, because all these reactions are reversible. With the exception of the longest-lived spectrum, the EAD-spectra in Figs. 2 and 3 represent, therefore, a mixture of these states. A target analysis, in which the data are fitted to a kinetic model, is necessary to obtain the pure spectra of the states, and then these spectra can be compared with the P^+/P , H_{D1}^-/H_{D1} , and Chl*/Chl and H*/H reference spectra to determine the nature of the formed states.

Target Analysis. The PSII RC contains eight excited states and at least two radical pair states (35–37), but including all these states separately in a model would be a step too far given the quality of our data and the information contained in it, because we only resolve four kinetic components. Instead, we use a five-compartmental model, depicted in Fig. 4a, that we have applied recently to describe the time-dependent spectral evolution of the PSII RC fluorescence (38). Because of the better signal-to-noise, the single ≈ 21 -ps component in the 681-nm mid-IR data was resolved in the Streak fluorescence experiment into two components of 6 and 36 ps, thus suggesting that a five-compartmental model is more appropriate. The model consists of two excited state compartments, one from which charge separation can occur (PC), one that transfers on a slow time scale to the other

H excited-state), we measured the spectrum of H^*/H in THF (see Fig. 2). In the H^*/H spectrum the ester band is weak relative to the keto band, and they shift from 1,746 to 1,739 cm^{-1} and from 1,708 to 1,686 cm^{-1} , respectively: the H^*/H spectrum behaves very similarly to Chl^*/Chl . Thus, the similarity of state RP1 with the steady-state H_{D1}^-/H_{D1} spectrum signifies that H_{D1}^- is formed after 0.6–0.8 ps. Note that on this time scale there is no P^+ formation; otherwise, the RP1 spectrum would be similar to the RP2 and RP3 spectra. Therefore, another Chl must act as the primary electron donor. Considering the location of Chl_{D1} between P_{D1} and H_{D1} (1–4), this electron donor must be pigment Chl_{D1} .

Heterogeneity of the Primary Electron Donor. Now that we have established the role of Chl_{D1} in the fast formation of a charge-separated pair, an alternative explanation for the slow “energy transfer” limited radical pair formation observed in previous studies (13, 15, 16, 38) as well as here presents itself: If the oxidation potential of this pigment is in some cases not sufficiently favorable to act as a fast electron donor to H_{D1} , the protein has to wait for P_{D1} to transfer an electron directly to H_{D1} , which is significantly slower because of the larger distance between them. The unfavorable redox potential of Chl_{D1} may be associated with a blue-shifted absorption of the Chl_{D1} chromophore, which would explain the long-lived, slightly blue-shifted emission that decays only in ≈ 30 ps into the state $P_{D1}^+H_{D1}^-$ (38). This alternative, heterogeneity-related explanation for the observed slow charge separation kinetics implies that the PC and BC compartments in Fig. 4 must be seen as situations occurring in different RCs and not as coexisting states in one RC.

Population of H_{D1}^- . We note that the time-evolution of the population of H_{D1}^- (see green line in Fig. 4b) is in good agreement with that recorded in the H Q_x region at room temperature by Greenfield *et al.* (16). Greenfield *et al.* fitted their data with an 8- and 50-ps time constant (comparable with our 6- and 36-ps time constants) but also found an instantaneous bleaching of $\approx 40\%$ of the final signal. It is conceivable that the subtraction of data from two different wavelengths, in combination with the strong solvent response around $t = 0$, has compromised their instrument response function (200 fs). Indeed, in an earlier publication without this treatment, an ≈ 1 -ps component in the increase of the H bleaching was found (14), comparable with our 0.6- to 0.8-ps component. Importantly, also in the Q_y region of the visible spectrum, the early formation of the radical pair may have been easily missed because the concentration of H_{D1}^- is only $\approx 20\%$ of the total excited states after 2 ps, because $\text{Chl}_{D1}^+H_{D1}^-$ is only a shallow trap. Therefore, it seems that our kinetic data are in good agreement with the data reported in literature but that due to the very specific signature of the H_{D1}^-/H_{D1} and P^+/P spectra in the mid-IR, we have succeeded in identifying the formation of a charge-separated state nearly isoenergetic with the excited state on a very early time scale.

Interpretation of the RP1 Difference Spectrum. The main band in the steady-state H_{D1}^-/H_{D1} spectrum is at $\approx 1,677$ cm^{-1} (29–31), suggesting that this band is due to the keto group of H_{D1} . Resonance Raman experiments in which the H are replaced by ^{13}C -OH-pheophytin put the keto of H_{D1} at 1,679 cm^{-1} (39), in agreement with this hypothesis. The RP1 spectrum differs from the H_{D1}^-/H_{D1} spectrum in the full development of the band at 1,687 cm^{-1} , which is only a weak shoulder in the latter, and therefore this band is a good candidate for the keto stretch of the Chl electron donor, Chl_{D1} . The concomitant positive band at 1,697 cm^{-1} seems a bit low for the keto stretch of the Chl cation, which in THF upshifts 25 cm^{-1} with respect to the neutral form, to 1,718 cm^{-1} (26). However, in the P^+ spectrum, the difference between the main bleach and the product band is also only 10

cm^{-1} . We propose, therefore, that Chl_{D1} has its keto stretch at $\approx 1,687$ cm^{-1} , suggesting a moderately strong hydrogen bond with the protein. An electrochromic band-shift probably leads to the presence of the Chl_{D1} band as a shoulder in the (steady state) H_{D1}^- spectrum. An alternative assignment for the Chl_{D1} keto stretch, however, is at 1,670 cm^{-1} , meaning that it is completely masked in our RP1 spectrum by the large positive (amide $\text{C}=\text{O}$) band at this frequency: The keto frequency of the triplet-carrying Chl at low temperature [either Chl_{D1} or Chl_{D2} (28, 40, 41)] has been reported to be at 1,670 cm^{-1} (28, 31). Because the low temperature triplet–singlet spectrum in the visible coincides with the band in the P^+/P spectrum assigned to Chl_{D1} (9), Diner and coworkers (9) proposed Chl_{D1} as the triplet carrying Chl.

Nature of the PC Excited State. The P^+/P state has a complicated spectrum (27–31) in which the contribution from several Chl/H molecules clearly can be seen. The high frequency of the main band at 1,704 cm^{-1} in the P^+/P spectrum is consistent with a keto $\text{C}=\text{O}$ group free from interactions with the protein. Possibly, the keto $\text{C}=\text{O}$ stretch of both P_{D1} and P_{D2} absorbs at 1,704 cm^{-1} , because the formation of Y_Z^+ (near P_{D1}) and Y_D^+ (near P_{D2}) both lead to a small spectral response at $\approx 1,704$ cm^{-1} (42–45). This analysis seems a likely interpretation because the cation state is localized mainly on P_{D1} (9), and the 1,704 cm^{-1} band has the largest amplitude in the P^+/P spectrum. The additional bands at 1,681, 1,670, and 1,653 cm^{-1} may be either due to electrochromic responses of nearby Chl, H, and amide $\text{C}=\text{O}$ molecules or reflect the partial localization of the cation on pigments other than P_{D1} , and in $\text{PC-P}^*/P$ reflect the delocalization of the excited state over several pigments. The responses at 1,681 and 1,670 cm^{-1} could be identified with the 1,687- and 1,675- cm^{-1} bands in the RP1 spectrum, which we tentatively identified with Chl_{D1} and H_{D1} , respectively (see above), if we take into account that electrochromic shifts and product bands to lower and higher energy, respectively, can cause a 6- cm^{-1} shift. Or, alternatively, the 1,670- cm^{-1} response may be due to Chl_{D1} (see above) and that at 1,681 cm^{-1} may be due to H_{D1} .

We can compare this tentative assignment of the $\text{PC-P}^*/P$ spectrum, which would indicate that the PC excited state is delocalized over P_{D1} , Chl_{D1} , and H_{D1} , with recent exciton calculations on the pigments in the PS2 RC: Novoderezhkin *et al.* (46) reported the lowest exciton state at ≈ 680 nm to be delocalized mainly over P_{D1} and Chl_{D1} , and over H_{D1} and Chl_{ZD1} , i.e., the pigments on the active branch of the RC, and charge separation from this state to be very fast, which is in good agreement with our assignments. However, the prediction of the calculations of Raszewski *et al.* (47) is that the lowest exciton states are localized on Chl_{D1} and H_{D2} , and the interpretation of P^+/P spectra of mutants of PS2 cores is that Chl_{D1} , Chl_{D2} , H_{D1} , and H_{D2} all absorb between 680 and 684 nm but that P_{D1} and P_{D2} absorb near 673 and 675 nm, respectively (9, 22). This finding makes it unlikely for P_{D1} to be populated to the high extent suggested here by the large amplitude of the 1,704- cm^{-1} bleach, invalidating either this realization of the low exciton states or the assignment of the 1,704- cm^{-1} band to P_{D1} . Conversely, we observe that the intense band at 1,704 cm^{-1} is missing in the BC spectrum. If we follow the assignment of the 1,704- cm^{-1} band to P_{D1} , then this result indicates that the BC excited state corresponds to the population of an exciton state that does not include P_{D1} , in agreement with the findings of Diner *et al.* (9, 22) and Raszewski *et al.* (47). The BC exciton state gives rise to slow charge separation, possibly, as suggested above, because of an unfavorable redox potential of Chl_{D1} in some RCs. However, to establish the connection between the PC/BC spectral differences, exciton states, and the decrease in rate of charge separation, a firm assignment of the bands in the mid-IR spectra is necessary, by means of site-directed mutagenesis.

Conclusion

We have studied the process of light-driven charge separation in the PSII RC of plants by using visible-pump-mid-IR-probe spectroscopy. Our analysis of the transient spectra and the detailed comparison with earlier measured steady-state P^+/P and H_{D1}^-/H_{D1} spectra show that whereas H_{D1}^- is formed after

0.6–0.8 ps, P^+ is not. Our data provide persuasive evidence that in the PSII RC Chl_{D1} is the initial electron donor, with H_{D1} as the acceptor.

This work was supported by the Netherlands Organization for Scientific Research, NWO-ALW.

1. Zouni, A., Witt, H. T., Kern, J., Fromme, P., Krauss, N., Saenger, W. & Orth, P. (2001) *Nature* **409**, 739–743.
2. Kamiya, N. & Shen, J. R. (2003) *Proc. Natl. Acad. Sci. USA* **100**, 98–103.
3. Ferreira, K. N., Iverson, T. M., Maghlaoui, K., Barber, J. & Iwata, S. (2004) *Science* **303**, 1831–1838.
4. Biesiadka, J., Loll, B., Kern, J., Irrgang, K. D. & Zouni, A. (2004) *Phys. Chem. Chem. Phys.* **6**, 4733–4736.
5. Nanba, O. & Satoh, K. (1987) *Proc. Natl. Acad. Sci. USA* **84**, 5730–5734.
6. Durrant, J. R., Klug, D. R., Kwa, S. L. S., Van Grondelle, R., Porter, G. & Dekker, J. P. (1995) *Proc. Natl. Acad. Sci. USA* **92**, 4798–4802.
7. Merry, S. A. P., Kumazaki, S., Tachibana, Y., Joseph, D. M., Porter, G., Yoshihara, K., Barber, J., Durrant, J. R. & Klug, D. R. (1996) *J. Phys. Chem.* **100**, 10469–10478.
8. Leegwater, J. A., Durrant, J. R. & Klug, D. R. (1997) *J. Phys. Chem. B* **101**, 7205–7210.
9. Diner, B. A., Schlodder, E., Nixon, P. J., Coleman, W. J., Rappaport, F., Lavergne, J., Vermaas, W. F. & Chisholm, D. A. (2001) *Biochemistry* **40**, 9265–9281.
10. Durrant, J. R., Hastings, G., Joseph, D. M., Barber, J., Porter, G. & Klug, D. R. (1992) *Proc. Natl. Acad. Sci. USA* **89**, 11632–11636.
11. Rech, T., Durrant, J. R., Joseph, D. M., Barber, J., Porter, G. & Klug, D. R. (1994) *Biochemistry* **33**, 14768–14774.
12. Klug, D. R., Rech, T., Joseph, D. M., Barber, J., Durrant, J. R. & Porter, G. (1995) *Chem. Phys.* **194**, 433–442.
13. Muller, M. G., Hucke, M., Reus, M. & Holzwarth, A. R. (1996) *J. Phys. Chem.* **100**, 9527–9536.
14. Greenfield, S. R., Seibert, M., Govindjee & Wasielewski, M. R. (1996) *Chem. Phys.* **210**, 279–295.
15. Groot, M. L., Van Mourik, F., Eijkelhoff, C., Van Stokkum, I. H. M., Dekker, J. P. & Van Grondelle, R. (1997) *Proc. Natl. Acad. Sci. USA* **94**, 4389–4394.
16. Greenfield, S. R., Seibert, M., Govindjee & Wasielewski, M. R. (1997) *J. Phys. Chem. B* **101**, 2251–2255.
17. Klug, D. R., Durrant, J. R. & Barber, J. (1998) *Philos. Trans. R. Soc. London A* **356**, 449–464.
18. Greenfield, S. R., Seibert, M. & Wasielewski, M. R. (1999) *J. Phys. Chem. B* **103**, 8364–8374.
19. Van Brederode, M. E., Van Mourik, F., Van Stokkum, I. H. M., Jones, M. R. & Van Grondelle, R. (1999) *Proc. Natl. Acad. Sci. USA* **96**, 2054–2059.
20. Van Brederode, M. E. & Van Grondelle, R. (1999) *FEBS Lett.* **455**, 1–7.
21. Van Brederode, M. E., Van Stokkum, I. H. M., Katilius, E., Van Mourik, F., Jones, M. R. & Van Grondelle, R. (1999) *Biochemistry* **38**, 7545–7555.
22. Diner, B. A. & Rappaport, F. (2002) *Annu. Rev. Plant Biol.* **53**, 551–580.
23. Barter, L. M. C., Durrant, J. R. & Klug, D. R. (2003) *Proc. Natl. Acad. Sci. USA* **100**, 946–951.
24. Frese, R. N., Germano, M., De Weerd, F. L., Van Stokkum, I. H. M., Shkuropatov, A. Y., Shuvalov, V. A., van Gorkom, H. J., van Grondelle, R. & Dekker, J. P. (2003) *Biochemistry* **42**, 9205–9213.
25. Prokhorenko, V. I. & Holzwarth, A. R. (2000) *J. Phys. Chem. B* **104**, 11563–11578.
26. Nabedryk, E., Leonhard, M., Mantele, W. & Breton, J. (1990) *Biochemistry* **29**, 3242–3247.
27. Breton, J., Hienerwadel, R. & Nabedryk, E. (1997) in *Spectroscopy of Biological Molecules: Modern Trends*, ed. Carmona, P. (Kluwer, Dordrecht, The Netherlands), pp. 101–106.
28. Noguchi, T., Tomo, T. & Inoue, Y. (1998) *Biochemistry* **37**, 13614–13625.
29. Tavitian, B. A., Nabedryk, E., Mantele, W. & Breton, J. (1986) *FEBS Lett.* **201**, 151–157.
30. Nabedryk, E., Andrianambinintsoa, S., Berger, G., Leonhard, M., Mantele, W. & Breton, J. (1990) *Biochim. Biophys. Acta* **1016**, 49–54.
31. Noguchi, T., Tomo, T. & Kato, C. (2001) *Biochemistry* **40**, 2176–2185.
32. Eijkelhoff, C., Van Roon, H., Groot, M. L., Van Grondelle, R. & Dekker, J. P. (1996) *Biochemistry* **35**, 12864–12872.
33. Van Stokkum, I. H. M., Larsen, D. S. & Van Grondelle, R. (2004) *Biochim. Biophys. Acta (Bioenerg.)* **1657**, 82–104.
34. Groot, M. L., Breton, J., van Wilderen, L., Dekker, J. P. & van Grondelle, R. (2004) *J. Phys. Chem. B* **108**, 8001–8006.
35. Groot, M. L., Peterman, E. J. G., Van Kan, P. J. M., Van Stokkum, I. H. M., Dekker, J. P. & Van Grondelle, R. (1994) *Biophys. J.* **67**, 318–330.
36. Booth, P. J., Crystall, B., Ahmad, I., Barber, J., Porter, G. & Klug, D. R. (1991) *Biochemistry* **30**, 7573–7586.
37. Konermann, L., Gatzert, G. & Holzwarth, A. R. (1997) *J. Phys. Chem. B* **101**, 2933–2944.
38. Van Mourik, F., Groot, M. L., Van Grondelle, R., Dekker, J. P. & Van Stokkum, I. H. M. (2004) *Phys. Chem. Chem. Phys.* **6**, 4820–4824.
39. Germano, M., Pascal, A., Shkuropatov, A. Y., Robert, B., Hoff, A. J. & van Gorkom, H. J. (2002) *Biochemistry* **41**, 11449–11455.
40. Kwa, S. L. S., Tilly, N. T., Eijkelhoff, C., Van Grondelle, R. & Dekker, J. P. (1994) *J. Phys. Chem.* **98**, 7712–7716.
41. Van Mieghem, F. J. E., Satoh, K. & Rutherford, A. W. (1991) *Biochim. Biophys. Acta* **1058**, 379–385.
42. Hienerwadel, R., Boussac, A., Breton, J. & Berthomieu, C. (1996) *Biochemistry* **35**, 15447–15460.
43. Hienerwadel, R., Boussac, A., Breton, J., Diner, B. A. & Berthomieu, C. (1997) *Biochemistry* **36**, 14712–14723.
44. Berthomieu, C., Hienerwadel, R., Boussac, A., Breton, J. & Diner, B. A. (1998) *Biochemistry* **37**, 10547–10554.
45. Zhang, H. M., Razeghifard, M. R., Fischer, G. & Wydrzynski, T. (1997) *Biochemistry* **36**, 11762–11768.
46. Novoderezhkin, V. I., Andrizhiyevskaya, E. G., Dekker, J. P. & Van Grondelle, R. (2005) *Biophys. J.*, in press.
47. Raszewski, G., Saenger, W. & Renger, T. (2005) *Biophys. J.* **88**, 986–998.